SolarPACES 2022, 28th International Conference on Concentrating Solar Power and Chemical Energy Systems
Receivers and Heat Transfer Media and Transport: Point Focus Systems
https://doi.org/10.52825/solarpaces.v1i.610

Published: 16 Apr. 2024

# Numerical Assessment of Enhanced Coatings in Wire Mesh Volumetric Absorbers

Antonio L. Avila-Marin[1][https://orcid.org/0000-0002-9523-9705], A. Morales[1][https://orcid.org/0000-0002-4690-1782], M. Farchado[1][https://orcid.org/0000-0002-8873-4556], G. San Vicente[1][https://orcid.org/0000-0002-3939-1630], M.E. Carra[2][https://orcid.org/0000-0001-5284-6938], J.A. Carballo[2][https://orcid.org/0000-0003-0529-5672], and D. Sanchez-Señoran[1][https://orcid.org/0000-0002-9891-5545]

[1] CIEMAT – Plataforma Solar de Almeria (PSA), Madrid, Spain

[2] CIEMAT – Plataforma Solar de Almeria (PSA), Tabernas-Almeria, Spain

**Abstract.** Two different wire mesh open volumetric receivers (OVRs) are studied together with six different coatings and two different working conditions in order to assess their effect on the performance of the OVR comparing them to the two baseline OVRs, uncoated and state-of-the-art. The results show that selective coatings produce the best OVR thermal results, having the best results when the solar absorptance is as high as possible and the thermal emittance is as low as possible.

**Keywords:** Volumetric Receiver, Volumetric Absorber, Selective Coating, Wire Mesh, LTNE, CFD.

## 1. Introduction

Among the different CSP technologies, central receiver systems (CRSs) do have the potential to increase the efficiency of the technology, make it more reliable and cost-effective, leading the future generation of CSP technologies. CRS can operate at very high temperatures and solar fluxes, and can be coupled with innovative power cycles and thermal energy storage (TES) systems, either commercially available or innovative ones [1, 2]. The most implemented CRS used molten nitrate salt technology, working at maximum temperatures of around 838K (565ºC). The hot molten salts are used to produce high-quality steam which drives a Rankine cycle to produce electricity [3].

Innovative new designs and alternatives to the reference tubular receivers are receiving research attention as possible solutions to increase solar-to-thermal/electrical efficiency, such as particle receivers [4], alternative point-focus designs [5] and volumetric receivers [6, 7]. Research on volumetric receiver's dates from the early 80s with the first volumetric concept proposed by Fricker [8]. Recent work has focused on the search for new designs and solutions for coupling open volumetric receivers (OVRs) with combined cycles [9]. Concerning the OVR, most of the literature studies deals with ceramic materials, as they withstand temperatures above 1073K [10]. However, new metallic designs are able to achieve high efficiencies for temperatures up to 1273K [11].

Moreover, CRSs usually paint the receivers with a non-selective coating in order to increase their solar absorptance ($\alpha_s$), despite those coatings having a high thermal emittance ($\varepsilon_T$). Currently, significant research is being devoted to the improvement of high-temperature selective coatings (SCs) that could work in air, which will allow their use in CRSs. The CIEMAT-

PSA has made some advances in this area, and this work will present data from two metal absorbers with six different coatings compared to two different baseline optical characteristics.

## 2. Baseline and coating descriptions

This work analyses how six different optical coatings affect the thermal performance of two metallic OVRs made of 310 stainless steel using a two-dimensional (2D) computational-fluid-dynamic (CFD) model, comparing the performance of the coatings against two baselines, uncoated and state-of-the-art. Two of the coatings have been developed by CIEMAT-PSA and are SCs. Another one is the commercial Pyromak 2500 coating. Finally, three cases involve theoretical candidates with intermediate values between the two SCs that may guide future materials development. In detail, the cases analysed are as follows:

- Case 1 (C1) refers to the baseline uncoated bare metallic mesh with the optical properties that have been validated with experiments and simulations: $\alpha_s = \varepsilon_T = 0.80$ [12].
- Case 2 (C2) adopts the state-of-the-art optical properties usually implemented in the numerical simulations, $\alpha_s = \varepsilon_T = 0.95$, for oxidized metals or bare ceramic materials [13, 14].
- Case 3 (C3) is an SC developed for high temperature applications where all layers are deposited using a dip-coating technique. It presents a $\alpha_s$ of 0.96 and a $\varepsilon_T$ of 0.16 at 973K. It is stable in air at temperatures up to 973K. It can be deposited on several stainless steel alloys and has the structure depicted in Figure 1.
- Case 4 (C4) represents a second SC using dip-coating technology, initially developed for application on silicon carbide and alumina substrates during the NEXTOWER Project [15], but which should be able to be applied to stainless steel absorbers. It has a solar absorptance of 0.973 and a thermal emittance of 0.652 at 973K. The coating was stable at 973K, however both optical properties were reduced due to high temperature layer contraction. The structure is shown in Figure 2.
- Case 5 (C5) is the Pyromark 2500 coating. It is used as the reference coating implemented in commercial tower power plants due to its high solar absorptance and good thermal durability. It is coated by spraying and cured following a specific thermal protocol and is stable up to 1366K. The solar absorptance varies from 0.96 to 0.97, depending on the layer thickness, and the thermal emittance at 973K is 0.878.
- Case 6 to 8 (C6–C8) have values that lie between SC1 (C3) and SC2 (C4) and help to provide a finer grained analysis of the effects of certain optical characteristics.

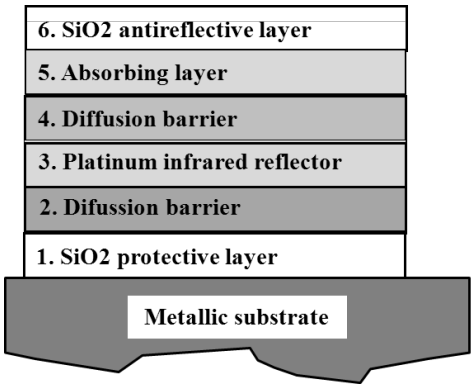


**Figure 1**. Layers of selective coatings designed for metallic receivers in CRSs

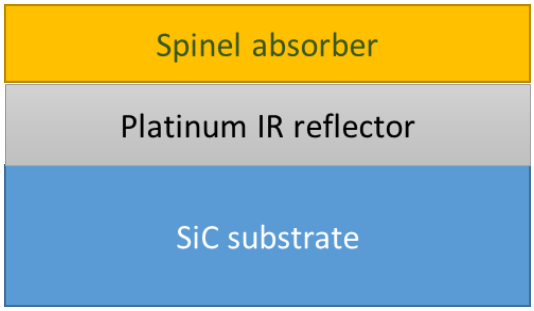


**Figure 2**. Layers of selective coating designed for ceramic receivers in CRSs

Figure 3 presents the thermal emittance variation with the temperature of the two SCs developed by CIEMAT-PSA, the commercial Pyromark and three theoretical selective candidates, while Table 1 presents the solar absorptance ($\alpha_s$) and the thermal emittance ($\varepsilon_T$) at 373 and 973K for those coatings and the two baseline OVRs.

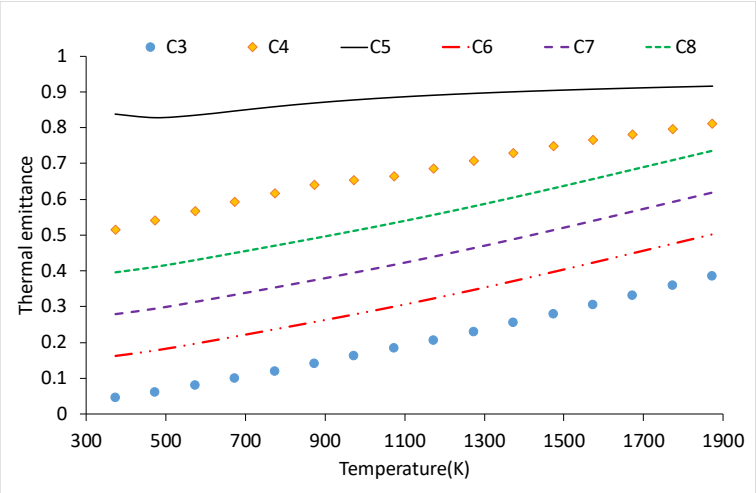


**Figure 3**. Thermal emittance of commercial Pyromark 2500, two selective coatings developed by CIEMAT-PSA and three theoretical selective coatings

**Table 1**. Main optical properties of the different cases analysed

| **Cases** | **C1** | **C2** | **C3** | **C4** | **C5** | **C6** | **C7** | **C8** |
|---|---|---|---|---|---|---|---|---|
| **Status** | Baseline | | Lab scale / Commercial | | | Theoretical | | |
| $\alpha_s$ | 0.80 | 0.95 | 0.960 | 0.973 | 0.960 | 0.963 | 0.967 | 0.970 |
| $\varepsilon_{373K}$ | | | 0.046 | 0.514 | 0.838 | 0.163 | 0.280 | 0.397 |
| $\varepsilon_{973K}$ | | | 0.162 | 0.652 | 0.878 | 0.279 | 0.396 | 0.513 |

## 3. Numerical methodology

The continuum method has been adopted in this research as it focuses on the macroscopic phenomena involved. This modelling strategy is usually adopted because of the balance between accuracy and low computational resources needed [16]. The main assumptions adopted are [17]: a) The air is an ideal gas; b) The flow is laminar; c) The thermal properties of the fluid and solid are temperature dependent; d) The radiative properties are isotropic; e) The incident radiation is collimated.

### 3.1. Conservative equations

Both phases (fluid and solid) energy equations have to be solved, especially when the temperature profiles of both phases are needed. In such a case, the local thermal non-equilibrium (LTNE) model is adopted, where the coefficient $h_v$ is responsible for coupling them.

$$\nabla\left(\langle\rho_f \; c_{p_f} \; T_f\rangle^f \;\; v_D\right) = \nabla\left(k_{eff,f}\,\nabla\,\langle T_f\rangle^f\right) + h_v\left(\langle T_s\rangle^f - \langle T_f\rangle^f\right) \quad (1)$$

$$0 = \nabla\left(k_{eff,s}\,\nabla\,\langle T_s\rangle^s\right) + h_v\left(\langle T_f\rangle^s - \langle T_s\rangle^s\right) - S_{rad} \quad (2)$$

The source term within the solid phase for the solar irradiation follows the Beer's law:

$$S_{rad} = a\,\beta\,I\,e^{-\beta\,z} \quad (3)$$

To analyse the effect of the radiation inside the OVR, the Rosseland approximation is used [18].

$$q_{rad} = -\frac{16 \cdot \sigma \cdot T_s^3}{3 \cdot \beta} \nabla \langle T_s \rangle^s \quad (4)$$

## 3.2. Effective properties

The effective properties are parameters required to solve the energy equations, and their accuracy determines the feasibility of the numerical predictions. The main properties are the heat transfer coefficient, $h_v$, the effective fluid and solid conductivities, $k_{eff,f}$ and $k_{eff,s}$, and the radiative properties, $\beta$.

### 3.2.1. Heat transfer coefficient

The heat transfer coefficient determines the rate of heat transferred from the solid porous structure to the fluid per unit volume and is the main parameter to couple both energy equations [19].

$$h_v = k_f \cdot \left(a \cdot Re_{d_h}^b \cdot Pr^c\right)/d_h^2 \quad (5)$$

### 3.2.2. Fluid and porous conductivities

The conduction is modelled with the correlations from [20].

$$k_{eff,f} = \emptyset \cdot k_f \quad (6)$$

$$k_{eff,s} = (1 - \emptyset) \cdot k_s/3 \quad (7)$$

### 3.2.3. Radiative properties

The main radiative property is the extinction coefficient which is dependent of the wire mesh diameter and the porosity following the next equation [12]:

$$\beta = \frac{8}{\pi} \cdot \frac{(1 - \emptyset)}{d} \quad (8)$$

## 3.3. Boundary conditions

The conservative equations require the following boundary conditions in order to be solved:

- The air temperature at the inlet boundary is fixed to 300 K together with a velocity of 1 m/s.
- The air pressure at the outlet boundary is set to 0.
- The thermal losses to the ambient are computed following the Stefan-Boltzmann law.

## 3.4. Wire mesh parameters

For the CFD simulations, two commercial wire mesh screens with a diameter of 50 mm and a thickness of 20 mm are used. Table 2 presents the main properties [21, 22]: d is the wire diameter, M is the mesh count, $\emptyset$ is the porosity, $a_v$ is the specific surface area and $\beta$ is the extinction coefficient. The coefficient a, b and c are those used in Equation (5).

**Table 2**. Alloy-310 wire meshes parameters

| Mesh type | d | M | ∅ | $a_v$ | $\beta$ | a | b | c |
|---|---|---|---|---|---|---|---|---|
| **A** | 1.00 | 0.20 | 70.1 | 1194 | 760 | 110.9 | 0.494 | 9.19 |
| **C** | 0.50 | 0.53 | 62.0 | 3044 | 1940 | 69.9 | 0.352 | 6.50 |

# 4. Results and discussion

Current SCs are able to work at temperatures up to 973K with a stable performance in air; however, OVRs require higher temperatures, especially for the solid phase of the volumetric receivers, which can reach temperatures of 1273K or higher. So, this study analyses two different working conditions, both having an inlet velocity of 1 m/s: a) the usual working conditions of OVRs of 600 kW/m$^2$ /s, and b) limiting the temperature of the solid phase to 973K.

## 4.1. Working condition 1: Solar flux equals 600 kW/m$^2$

This section studies two metallic OVRs (Table 2) with 70% and 62% porosity, with eight different optical properties (Figure 3 and Table 1) and a solar flux of 600 kW/m$^2$.

Table 3 presents the main thermal results for the first working condition (WC1). It is worth noting that in all the cases, except C1, the frontal solid temperature ($T_{s-in}$) for both meshes exceeds the 973K limit for SCs.

Overall, the increase in $\alpha_s$ means a higher solid temperature, and a higher air outlet temperature ($T_{f-out}$), while the decrease of $\varepsilon_T$ with temperature results in lower radiative thermal losses (Loss) of the OVR frontal surface, which subsequently yields higher thermal efficiency ($\eta_{OVR}$). Thus, comparing C1 and C2, where both optical parameters ($\alpha_s, \varepsilon_T$) change from 0.80 to 0.95, higher $T_{s-in}$ and thermal losses (Loss) are observed, but an improvement of $T_{f-out}$ and $\eta_{OVR}$ is also seen due to a higher $\alpha_s$ and despite the higher thermal losses. If C1 (uncoated material) is compared to C5 (Pyromark), the relative thermal efficiency improvement ($\Delta\eta_{OVR}$) is 17%. Comparing with the different SCs, the better the optical properties ($\uparrow \alpha_s$ and $\downarrow \varepsilon_T$), the better the thermal efficiency. It should also be noted that the better the thermal efficiency, the higher $T_{s-in}$ and $T_{f-out}$.

Finally, the thermal performance of a stainless steel OVR can be improved greatly using a non-selective coating such as Pyromark 2500 (17%), and even more if a SC is used, ranging from 20.1 to 24.8%. Between the two mesh types (A & C), the results are better for mesh C, with the $\Delta\eta_{OVR}$ of the different cases being similar. The value for mesh type C is slightly lower since the uncoated mesh (C1) has better performance, which makes the $\Delta\eta_{OVR}$ lower. However, it is important to note that mesh type C could reach an efficiency of 89.6% with the Pyromark coating and even 92.3% with the first SC (C3).

**Table 3**. Working conditions 1 – Thermal results of OVRs with meshes A and C for the eight different cases studied

| **Cases** | **C1** | **C2** | **C3** | **C4** | **C5** | **C6** | **C7** | **C8** |
|---|---|---|---|---|---|---|---|---|
| **Status** | Baseline | | Lab scale / Commercial | | | Theoretical | | |
| **Mesh type A** | | | | | | | | |
| $\mathbf{T_{f-out}}$, (K) | 664 | 717 | 750 | 734 | 722 | 746 | 742 | 738 |
| $\mathbf{T_{s-in}}$, (K) | 935 | 1016 | 1085 | 1048 | 1026 | 1075 | 1066 | 1057 |
| **Loss**, $(\mathbf{kW/m^2})$ | -34.3 | -57.0 | -19.6 | -48.7 | -55.9 | -27.5 | -34.9 | -41.8 |
| $\boldsymbol{\eta_{OVR}}$, (%) | 73.5 | 84.6 | 91.8 | 88.3 | 85.8 | 90.8 | 89.9 | 89.1 |
| $\boldsymbol{\Delta\eta_{OVR}}$, (%) | 0.0 | 15.1 | 24.8 | 20.1 | 16.7 | 23.5 | 22.4 | 21.2 |

| Mesh type C | | | | | | | | |
|---|---|---|---|---|---|---|---|---|
| $\mathbf{T_{f-out}}$, (K) | 673 | 735 | 753 | 749 | 740 | 752 | 752 | 751 |
| $\mathbf{T_{s-in}}$, (K) | 744 | 814 | 838 | 832 | 820 | 836 | 835 | 833 |
| **Loss**, $(\mathbf{kW/m^2})$ | -13.6 | -23.2 | -5.3 | -18.0 | -22.4 | -8.4 | -11.5 | -14.6 |
| $\boldsymbol{\eta_{OVR}}$, (%) | 75.5 | 88.5 | 92.3 | 91.5 | 89.6 | 92.1 | 92.0 | 91.8 |
| $\Delta\boldsymbol{\eta_{OVR}}$, (%) | 0.0 | 17.2 | 22.4 | 21.3 | 18.7 | 22.1 | 21.9 | 21.6 |

## 4.2. Working condition 2: Variable solar flux

Given that the constant solar flux of 600 kW/m$^2$ produced $T_{s-in}$ above 973K, which is the current limit for selective coatings, in all but the baseline case, this working condition adjusted incident solar fluxes to limit the temperatures for all eight cases to that maximum.

Table 4 presents the main thermal results for the second working condition (WC2). It is worth noting that the solar flux (Flux) of all the cases with mesh type A, except C1, have a value lower than 600 kW/m$^2$ to achieve the target $T_{s-in}$. On the other hand, all the cases with mesh type C require a much higher Flux value to achieve the same target temperature.

The cases with mesh A have a $T_{f-out}$ ranging from 681 to 690K, while $\eta_{OVR}$ varies from 73.0 to 92.8% and the incident solar flux varies from 499 to 646 kW/m$^2$. The cases with mesh C have a $T_{f-out}$ ranging from 874 to 878K, while $\eta_{OVR}$ varies from 73.6 to 91.8 % and the incident solar flux varies from 499 to 971 kW/m$^2$. The OVRs with mesh C have a higher $T_{f-out}$, ~200K greater, than OVRs with mesh A, despite the $\eta_{OVR}$ having similar values. In some cases $\eta_{OVR}$ has higher values for mesh type A (C3; C6; C7), while in other cases OVRs with mesh type C have higher values (C1; C2; C4; C5; C8).

Moreover, the thermal losses are almost the same in all cases for both mesh types, because they have the same $T_{s-in}$, and the same optical properties, only varying in their physical properties (Table 2), which are similar in terms of ∅.

**Table 4**. Working conditions 2 – Thermal results of OVRs with meshes A and C for the eight different cases analysed

| Cases | C1 | C2 | C3 | C4 | C5 | C6 | C7 | C8 |
|---|---|---|---|---|---|---|---|---|
| **Status** | Commercial / Available at lab scale | | | | | Theoretical | | |
| **Mesh type A** | | | | | | | | |
| $\mathbf{T_{f-out}}$, (K) | 688 | 690 | 681 | 687 | 689 | 682 | 684 | 685 |
| **Flux**, $(\mathbf{kW/m^2})$ | 646 | 554 | 499 | 525 | 544 | 505 | 511 | 517 |
| **Loss**, $(\mathbf{kW/m^2})$ | -40.4 | -48.0 | -11.3 | -35.6 | -45.1 | -17.1 | -23.1 | -28.9 |
| $\boldsymbol{\eta_{OVR}}$, (%) | 73.0 | 85.5 | 92.8 | 89.6 | 86.8 | 91.9 | 91.2 | 90.5 |
| $\Delta\boldsymbol{\eta_{OVR}}$, (%) | 0.0 | 17.1 | 27.1 | 22.8 | 18.9 | 26.0 | 25.0 | 23.9 |
| **Mesh type C** | | | | | | | | |
| $\mathbf{T_{f-out}}$, (K) | 877 | 878 | 874 | 876 | 877 | 875 | 875 | 876 |
| **Flux**, $(\mathbf{kW/m^2})$ | 971 | 827 | 774 | 792 | 814 | 779 | 782 | 787 |
| **Loss**, $(\mathbf{kW/m^2})$ | -40.4 | -47.9 | -11.3 | -35.4 | -45.0 | -17.2 | -23.1 | -29.0 |
| $\boldsymbol{\eta_{OVR}}$, (%) | 73.6 | 86.6 | 91.8 | 90.1 | 87.8 | 91.3 | 91.0 | 90.6 |
| $\Delta\boldsymbol{\eta_{OVR}}$, (%) | 0.0 | 17.6 | 24.6 | 22.4 | 19.3 | 24.1 | 23.6 | 23.0 |

# 5. Conclusions

This numerical research analyses the performance of open volumetric receivers with two different designs and how they vary for eight different optical properties. It includes the optical properties of uncoated wire mesh screens, the usual properties adopted in numerical simula-

tions ($\alpha_s = \varepsilon_T = 0.95$), two selective coatings developed by CIEMAT-PSA, the commercial Pyromark 2500, together with three theoretical selective coatings. Moreover, two different working conditions have been adopted to account for the usual working conditions implemented for OVRs, taking into consideration the current temperature limit for the feasibility and stability of selective coatings in air. In summary, OVRs with mesh type C and a porosity of 62% tend to perform better than the OVRs with mesh type A. Concerning the different optical properties studied, the higher the solar absorptance and the lower the thermal emittance, the better the results, as happens with the selective coatings developed by CIEMAT-PSA. The best performance corresponds to the selective coating (case 3) with a solar absorptance of 0.96 and a thermal emittance of 0.16 at 973K, with an improvement with respect to the uncoated material (case 1) ranging from 22 to 27%. On the other hand, the improvement with the commercial Pyromark paint (case 5) varies from 17 to 19%. Despite the fact that using a selective coating clearly enhances OVR performance, further development of better coatings that can work at higher temperatures is required in order to increase the current temperature limit.

## Data availability statement

The data supporting the results of this article can be accessed upon request to the authors.

## Author contributions

**Antonio L. Avila-Marin**: Conceptualization, Investigation, Software, Data curation, Methodology, Formal Analysis, Resources, Writing – original draft, Visualization; **A. Morales**: Investigation, Data curation, Funding acquisition, Formal Analysis, Writing – review & editing; **M. Farchado**: Investigation, Data curation, Formal Analysis, Writing – review & editing; **G. San Vicente**: Investigation, Data curation, Formal Analysis, Writing – review & editing; **M.E. Carra**: Investigation, Software, Resources, Writing – review & editing; **J.A. Carballo**: Investigation, Software, Resources, Formal Analysis, Writing – review & editing; **D. Sanchez-Señoran**: Investigation, Software, Resources, Formal Analysis, Writing – review & editing;

## Competing interests

The authors declare no competing interests.

## Funding

This work has been funded by the National R+ D+ i Plan Project SOLTERMIN, ENE2017-83973-R, of the Spanish Ministry of Science and Innovation (co-funded with European Regional Development funding).

## References

1. C.K. Ho, Advances in central receivers for concentrating solar applications, Sol Energy 152 (2017) 38-56. https://doi.org/10.1016/j.solener.2017.03.048.
2. Y.-L. He, Y. Qiu, K. Wang, F. Yuan, W.-Q. Wang, M.-J. Li, J.-Q. Guo, Perspective of concentrating solar power, Energy 198 (2020) 117373. https://doi.org/10.1016/j.energy.2020.117373.
3. A.L. Avila-Marin, J. Fernandez-Reche, F.M. Tellez, Evaluation of the potential of central receiver solar power plants: Configuration, optimization and trends, Appl Energy 112 (2013) 274-288. https://doi.org/10.1016/j.apenergy.2013.05.049.
4. C.K. Ho, A review of high-temperature particle receivers for concentrating solar power, Appl Therm Eng 109 (2016) 958-969. https://doi.org/10.1016/j.applthermaleng.2016.04.103.

5. M. Cagnoli, J.J. Falsig, I. Pagola, A. Peña-Lapuente, M. Sanchez, L. Savoldi, C. Villasante, R. Zanino, Design methodology for a prototype helical receiver adopted in the MOSAIC solar bowl system, Sol Energy 208 (2020) 905-916. https://doi.org/10.1016/j.solener.2020.08.012.
6. F. Zaversky, L. Aldaz, M. Sánchez, A.L. Ávila-Marín, M.I. Roldán, J. Fernández-Reche, A. Füssel, W. Beckert, J. Adler, Numerical and experimental evaluation and optimization of ceramic foam as solar absorber – Single-layer vs multi-layer configurations, Appl Energy 210 (2018) 351-375. https://doi.org/10.1016/j.apenergy.2017.11.003.
7. A.L. Avila-Marin, J. Fernandez-Reche, S. Gianella, L. Ferrari, D. Sanchez-Señoran, Experimental study of innovative periodic cellular structures as air volumetric absorbers, Renew Energy 184 (2022) 391-404. https://doi.org/10.1016/j.renene.2021.11.021.
8. H.W. Fricker, Proposal for a novel type of solar gas receiver, Proceedings of the International Seminar on Solar Thermal Heat Production, Stuttgart, Germany, 1983.
9. F. Zaversky, I. Les, P. Sorbet, M. Sánchez, B. Valentin, J.-F. Brau, F. Siros, The challenge of solar powered combined cycles – Providing dispatchability and increasing efficiency by integrating the open volumetric air receiver technology, Energy 194 (2020) 116796. https://doi.org/10.1016/j.energy.2019.116796.
10. A.L. Avila-Marin, Volumetric receivers in solar thermal power plants with central receiver system technology: A review, Sol Energy 85(5) (2011) 891-910. https://doi.org/10.1016/j.solener.2011.02.002.
11. M. Livshits, L. Avivi, A. Kribus, Dense wire mesh as a high-efficiency solar volumetric absorber, In: Proceedings of the ASME Summer Heat Transfer Conference, Bellevue, Washington, USA, 2017.
12. A.L. Avila-Marin, C. Caliot, M. Alvarez de Lara, J. Fernandez-Reche, M.J. Montes, A. Martinez-Tarifa, Homogeneous equivalent model coupled with P1-approximation for dense wire meshes volumetric air receivers, Renew Energy 135 (2019) 908-919. https://doi.org/10.1016/j.renene.2018.12.061.
13. A.L. Avila-Marin, CFD parametric analysis of wire meshes open volumetric receivers with axial-varied porosity and comparison with small-scale solar receiver tests, Renew Energy 193 (2022) 1094-1105. https://doi.org/10.1016/j.renene.2022.05.060.
14. Z. Wu, C. Caliot, G. Flamant, Z. Wang, Coupled radiation and flow modeling in ceramic foam volumetric solar air receivers, Sol Energy 85(9) (2011) 2374-2385. https://doi.org/10.1016/j.solener.2011.06.030.
15. A. Rinaldi, Advanced Material solutions for next generation high efficiency concentrated solar power (CSP) tower systems-NEXTOWER. H2020 Programme. Contract number: 721045, (2017).
16. A.L. Avila-Marin, J. Fernandez-Reche, A. Martinez-Tarifa, Modelling strategies for porous structures as solar receivers in central receiver systems: A review, Renew Sustain Energy Rev 111 (2019) 15-33. https://doi.org/10.1016/j.rser.2019.03.059.
17. A.L. Avila-Marin, J. Fernandez-Reche, C. Caliot, A. Martinez-Tarifa, M.A.d. Lara, CFD numerical model for open volumetric receivers with graded porosity dense wire meshes and experimental validation, AIP Conf Proc 2126(1) (2019) 030005. https://doi.org/10.1063/1.5117517.
18. S. Du, T. Xia, Y.-L. He, Z.-Y. Li, D. Li, X.-Q. Xie, Experiment and optimization study on the radial graded porous volumetric solar receiver matching non-uniform solar flux distribution, Appl Energy 275 (2020) 115343. https://doi.org/10.1016/j.apenergy.2020.115343.
19. A.L. Avila-Marin, C. Caliot, G. Flamant, M. Alvarez de Lara, J. Fernandez-Reche, Numerical determination of the heat transfer coefficient for volumetric air receivers with wire meshes, Sol Energy 162 (2018) 317-329. https://doi.org/10.1016/j.solener.2018.01.034.
20. M.A. Schuetz, L.R. Glicksman, A Basic Study of Heat Transfer Through Foam Insulation, J Cell Plast 20(2) (1984) 114-121. https://doi.org/10.1177/0021955x8402000203.
21. A.L. Avila-Marin, M. Alvarez-Lara, J. Fernandez-Reche, Experimental results of gradual porosity wire mesh absorber for volumetric receivers, Energy Procedia 49 (2014) 275-283. https://doi.org/10.1016/j.egypro.2014.03.030.

22. A.L. Avila-Marin, M. Alvarez de Lara, J. Fernandez-Reche, Experimental results of gradual porosity volumetric air receivers with wire meshes, Renew Energy 122 (2018) 339-353. https://doi.org/10.1016/j.renene.2018.01.073.